N91-21193

SLIDING MODE CONTROL of MAGNETIC SUSPENSIONS for PRECISION POINTING and TRACKING APPLICATIONS

Kathleen M. Misovec, Frederick J. Flynn, Bruce G. Johnson
SatCon Technology Corporation
12 Emily Street
Cambridge
MA 02139-4507

J. Karl Hedrick
University of California at Berkeley
Berkeley
CA 94720

SLIDING MODE CONTROL OF MAGNETIC SUSPENSIONS FOR PRECISION POINTING AND TRACKING APPLICATIONS

Kathleen M. Misovec, SatCon Technology Corporation, Cambridge, MA

Frederick J. Flynn, SatCon Technology Corporation, Cambridge, MA

Bruce G. Johnson, SatCon Technology Corporation, Cambridge, MA

J. Karl Hedrick, Prof. of Mechanical Engineering, University of California at Berkeley, Berkeley, CA

Presented at: Workshop on Aerospace Applications of Magnetic Suspension Technology
NASA Langley Research Center, Hampton, VA; Sept. 25, 1990

ABSTRACT

This paper examines a recently developed nonlinear control method, sliding mode control, as a means of advancing the achievable performance of space-based precision pointing and tracking systems that use nonlinear magnetic actuators. The appeal of sliding mode control is its direct treatment of system nonlinearities. Analytic results indicate that sliding mode control improves performance compared to linear control approaches. In order to realize these performance improvements, precise knowledge of the plant is required. Additionally, the interaction of an estimation scheme and the sliding mode controller has not been fully examined in the literature. Estimation schemes were designed for use with this sliding mode controller that do not seriously degrade system performance. We designed and built a laboratory testbed to determine the feasibility of utilizing sliding mode control in these types of applications. Using this testbed, experimental verification of our analyses is ongoing.

INTRODUCTION

Space-based precision pointing and tracking systems typically operate in environments that require high levels of vibration isolation to achieve desired tracking performance. Consider the system illustrated in Fig. 1. The "tracking body" could be a telescope or a laser. The tracking body must rapidly point from target to target, a maneuver commonly referred to as slewing. A one meter diameter target located 10,000 km from the tracking body mandates slewing accuracies on the order of 100 nanoradians. The tracking body, however, is attached to a vibrating space structure. Disturbance vibrations are typically caused by machinery on the space structure. Any disturbance vibration that is transmitted to the tracking body can cause imprecision in the slewing

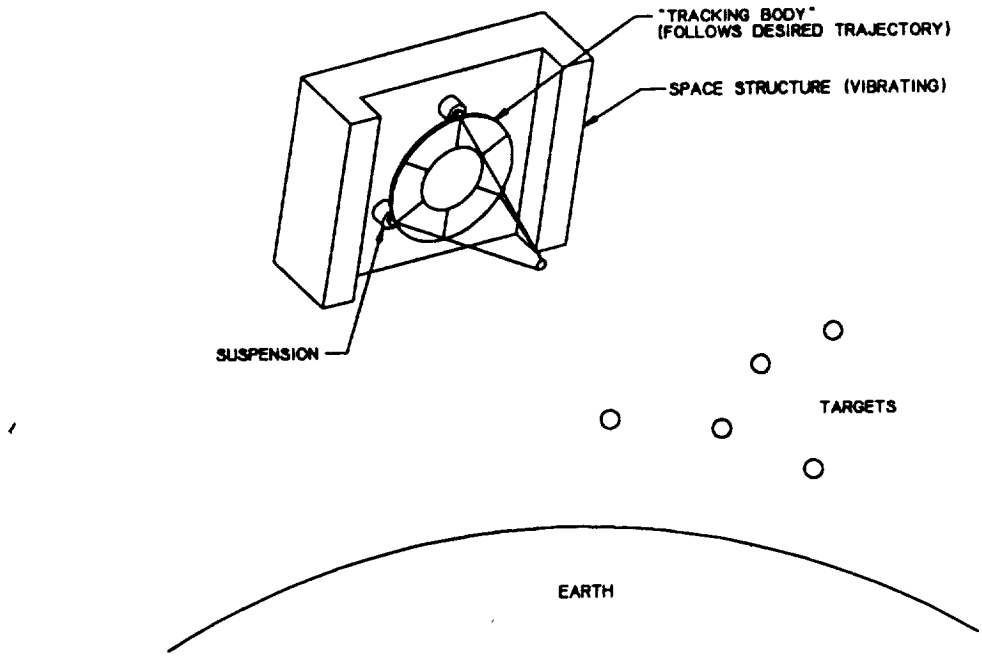

Figure 1. Space-Based Precision Pointing and Tracking

maneuver. Even a small amount of disturbance vibration can be catastrophic to the mission because the slewing requirements are extremely stringent. For example, the SAVI (Space Active Vibration Isolation) program is an earth-based full-scale test-bed of a magnetic suspension for pointing and slewing a 6000 kg mirror. Specifications are 80 db of isolation from 1 Hz to 2 kHz (6).

Nonlinear magnetic actuators, because of their high force per mass capability, are a promising means of achieving the required isolation while providing forces or torques for slewing. An inherent feature of the actuators, however, is coupling between the magnetic gap and the force. This coupling produces an undesirable path between disturbance vibrations and precision tracking forces. To date, vibration isolation systems utilizing these actuators face limitations on achievable isolation, especially under load, if slewing.

The actuators consist of a ferromagnetic material wrapped with a current-carrying coil (Fig. 2). Ferromagnetic material is also attached to the tracking body. An attractive force is exerted by the actuator on the tracking body. An equal and opposite force is exerted by the tracking body on the space structure, but this effect is negligible because the space structure is typically much more massive than the tracking body. Because the force on the tracking body is attractive force only, two actuators per degree of freedom are required. Force couples produce control torques. To first order, the force is proportional to the square of the ratio of current to gap. Thus, it is nonlinear in both current and gap. Another interesting feature is that the actuator is open-loop unstable. Indeed if the tracking body is initially in equilibrium at the centered position with equal currents in the actuators, and it is perturbed towards one of the actuators, at fixed current, the attractive force toward this actuator will increase, which is a destabilizing effect. We can also see this effect if we linearize the force-gap-current relation as is shown in the figure. For

destabilizing force proportional to the displacement. For the suspension system, there is an associated unstable frequency determined by the unstable spring stiffness and the tracking body mass.

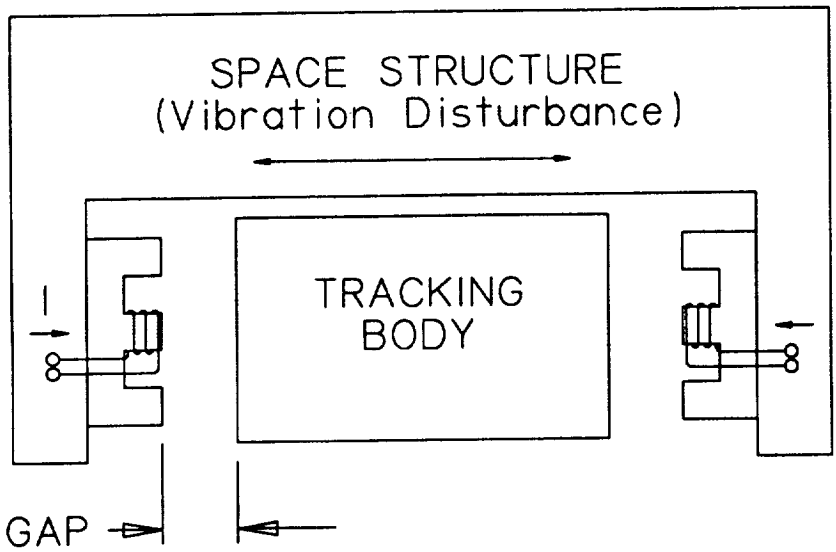

$$F \propto \frac{I^2}{gap^2} \propto B^2$$

$$F = -K_G \, \Delta gap + K_I \, \Delta I$$

Figure 2. Electromagnetic Actuator

A variety of options are available for use in the control of this type of magnetic suspension. These include gap feedback, flux feedback, and force feedback. Flux feedback is being used in the SAVI program. The motivation in this type of control scheme is the fact that when the force is linearized about a bias flux, the relationship between incremental force and flux is linear. The primary drawback of this approach arises because the flux sensor measures flux at the point where the sensor is located. In reality, the flux varies along the face of the actuators, and this variation looks like a modelling error in the flux-force relationship. This in turn may increase the tracking (slewing) error of the system. Gap sensors, on the other hand can give very precise information about the force because the precise gap sensors are available and the geometry of the actuator is fixed and known. However, as shown, the relationship between force, current and gap is nonlinear. The linearized relationship can be used in a linear control system such as the one shown in Fig. 3. A linear control system with inertial position feedback, however, can not meet the strict specifications of this type of problem. An examination of a linear control approach will illustrate the engineering difficulties of precision pointing and tracking systems. Space structure vibration is an output disturbance to this control system. Space structure motion (disturbance vibration) changes the gap between the structure and the tracking body causing an undesirable path, via the actuator, between the vibration disturbance and inertial position. In these applications, broad frequency range disturbances are present up to typical closed loop system bandwidths.

Figure 3. Block Diagram of Phase Lead Controller

At the open loop crossover frequency, the magnitude of the transfer function between inertial position and disturbance is dependent only on the unstable spring frequency and the crossover frequency, independent of the type of linear controller. The magnitude of this transfer function should be small for good tracking performance. As Eq. (1) shows, we have two options, increase the crossover frequency of the system or decrease the spring frequency.

$$\text{At crossover } (\omega_C) \quad \frac{\text{Position}}{\text{Disturbance}} = \frac{\omega_U^2}{2(\omega_U^2 + \omega_C^2)} \tag{1}$$

ω_U = Actuator unstable frequency
ω_C = Crossover frequency

The problem is that we are limited in both of these options. More precisely, the unstable spring frequency, which is a result of the coupling between force and gap can not be decreased indefinitely because of limitations on actuator power and size. The crossover frequency is limited as well by system bandwidth constraints. For example in the SAVI program, flexible structure modes of the mirror support structure start at 10-15 Hz. A control system with a higher bandwidth would excite these modes and is therefore undesirable. The key point is that for the vibration isolation levels required for many types of precision pointing and tracking systems, it is impossible to meet the specifications with linear controllers.

We examined sliding mode control, a recently developed nonlinear control method (5,2), as an alternative approach that has the potential to achieve higher levels of performance than are currently attainable. Fig. 4 is a rather complicated block diagram illustrating the sliding mode approach. The control goal is to have the tracking body (plant) follow a desired (reference) inertial trajectory. Nonlinear magnetic actuators produce forces on the plant changing it's inertial position. Vibration disturbances of the space structure change the gap between the tracking body and the space structure

producing the undesirable vibration path between vibration disturbance and inertial position. The sliding mode controller has the potential to achieve better performance than linear controllers because it's structure directly compensates for this vibration path. A set of control forces is calculated based on the difference between the estimated inertial state and the desired inertial state. A feedfoward term is also included. Gap sensor measurements are used in a nonlinear plant inversion of the gap-force-current relation to obtain control currents.

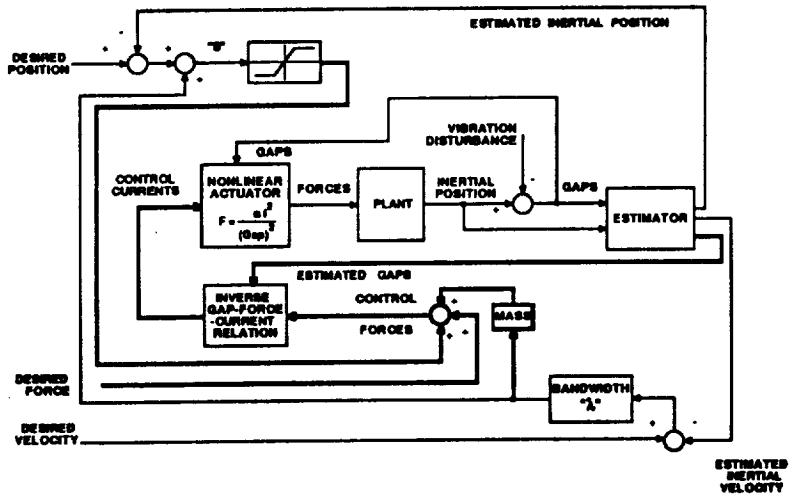

Figure 4. Sliding Mode Control Block Diagram

Lyaponov analysis guarantees that the controller with perfect state feedback will be stable in the presence of bounded modelling uncertainty and disturbances. The sliding mode control "balance condition" approximates the tracking error along a certain trajectory and is dependent on the modelling uncertainty bounds. The aim of the controller is to cancel out the effects of the unwanted vibration disturbance path. While the sliding mode control structure eliminates the weaknesses in the linear control approach, for high levels of performance, this approach depends strongly on having highly accurate plant models as well as precise measurement devices and a well-designed estimation scheme.

TEST-BED DESCRIPTION AND SYSTEM MODELLING

Testbed Description

The goal of the testbed is to capture the important features of the space-based precision pointing and tracking application in earth-based, laboratory-sized hardware. As shown in Fig. 5, the tracking body consists of a 7 kg mass supported on an air table, which eliminates the gravity-biasing effects. This mass, which will be called the isolated mass, has three degrees of freedom; two translational labelled x and y and one angular, labelled Θ. Magnetic actuators that produce forces on the isolated mass are mounted on moving rails. Four E-core actuators are used for both translational x (tracking/slew) direction and for the angular θ direction. Two pot core actuators are used to provide

forces in the ± y direction. Sensors include gap sensors, an angular velocity sensor, an accelerometer, and LVDT rail position sensors (7).

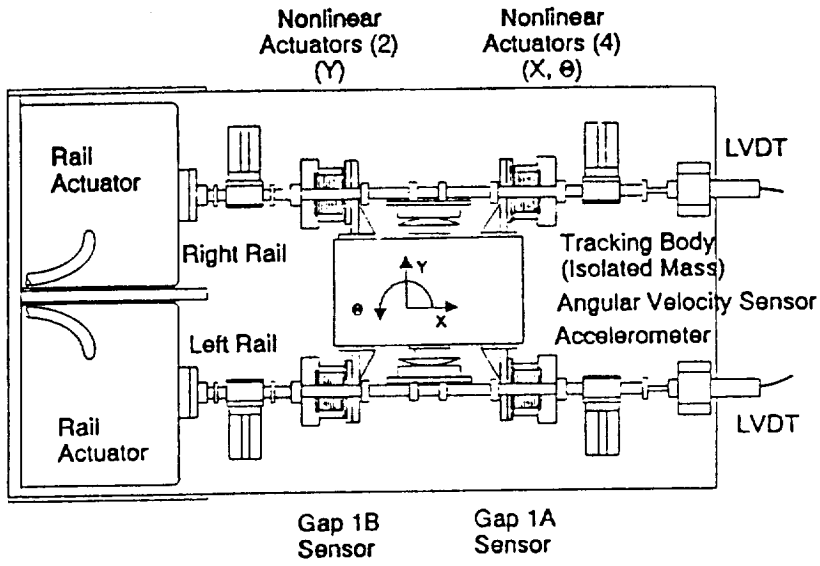

Figure 5. Top View of Testbed

The baseline test scenario consists of large amplitude (many times the nominal magnetic gap), low frequency motion in the x-direction. The moving rails, under separate linear position control loops, simulate the vibrating space structure in addition to allowing the slew motion. Disturbance vibrations can be introduced in the x and θ directions. Angular disturbances are input by differentially exciting the rails. Simulation results in this paper consist of single frequency tracking under the presence of a single frequency angular vibration disturbance. Broadband disturbances should be considered at a later time with the acquisition of a better angular sensor. Performance measures of rms tracking error and vibration isolation are considered.

System Modelling: Dynamics

By applying Newton's laws, we can obtain the dynamic equations of motion of the isolated mass (Eq. (2), (3), and (4)).

$$m\ddot{x} = (F_{1A} - F_{1B}) + (F_{2A} - F_{2B})$$

$$= \left(\frac{\alpha_x I_{1A}^2}{2(g_{1A}+C_x)^2} - \frac{\alpha_x I_{1B}^2}{2(g_{1B}+C_x)^2} \right) \tag{2}$$

$$+ \left(\frac{\alpha_x I_{2A}^2}{2(g_{2A}+C_x)^2} - \frac{\alpha_x I_{2B}^2}{2(g_{2B}+C_x)^2} \right)$$

$$I\ddot{\theta} = L\,(F_{1A}-F_{1B}) - L\,(F_{2A} - F_{2B})$$

$$= L\left(\frac{\alpha_x I_{1A}^2}{2(g_{1A}+C_x)^2} - \frac{\alpha_x I_{1B}^2}{2(g_{1B}+C_x)^2} \right) \tag{3}$$

$$- L\left(\frac{\alpha_x I_{2A}^2}{2(g_{2A}+C_x)^2} - \frac{\alpha_x I_{2B}^2}{2(g_{2B}+C_x)^2} \right)$$

$$m\ddot{y} = F_{3A} - F_{3B}$$

$$= \frac{\alpha_y I_{3A}^2}{2(g_{3A}+C_y)^2} - \frac{\alpha_y}{2} \frac{I_{3B}^2}{(g_{3B}+C_y)^2} \tag{4}$$

where

m	= mass
I	= Moment of inertia
F_{1A}	= Force actuator 1A
I_{1A}	= Current actuator 1A
g_{1A}	= Gap actuator 1A
C_x	= Modelling constant
L	= Moment arm (m)

The controller for the slew (x) direction and the angular (θ) direction is designed as if they were decoupled. This is due to the fact that there are more inputs than degrees of freedom. Referring to Eq. (2) and (3), we see the slew direction is controlled by an addition of (F_{1A} - F_{1B}) and (F_{2A} - F_{2B}) while angle θ as controlled by the difference. The y axis is decoupled from both the x and the θ axes.

Based on more detailed magnetic actuator modelling as well as experimental actuator testing, the x, θ axis actuator models are accurate to within 1% for the range of gaps we run in our experiments. This bound is used in the sliding mode controller design (7).

System Modelling: Kinematics

Kinematic relationships are used in the estimation scheme. At low frequencies, the accelerometer and angular velocity sensor do not provide good information. Low frequency state estimates can be obtained based on gap sensor and LVDT rail measurements by manipulating the kinematic relationships presented below.

A schematic representation of the test-bed geometry at two different positions of the isolated mass and rails is shown in Fig. 6. Small angle approximations are used to obtain the following relations. An expression for each gap can be obtained in terms of inertial position of the isolated mass, x, the inertial angular position of the isolated mass, θ, the nominal (centered) gap, g_0 and a position of the associated linear actuator rail, x_{LAL} or x_{LAR} (Eq. (5-8)).

$$g_{1A} = (x_{LAL}+g_0) - (x + L\theta) \tag{5}$$

$$g_{1B} = -(x_{LAL} - g_0) + (x + L\theta) \tag{6}$$

$$g_{2A} = (x_{LAR} + g_0) - (x - L\theta) \tag{7}$$

$$g_{2B} = (x - L\theta) - (x_{LAR} - g_0) \tag{8}$$

SLIDING MODE CONTROLLER DESIGN

The controller must choose six currents based on gap measurements, position errors, velocity errors and desired accelerations. Following the standard sliding mode control approach (2,5), a sliding surface, s is defined for each degree of freedom (Eq. (9-11)).

$$s_x = (\dot{x} - \dot{x}_d) + \lambda(x - x_d) \tag{9}$$

$$s_\theta = (\dot{\theta} - \dot{\theta}_d) + \lambda(\theta - \theta_d) \tag{10}$$

$$s_y = (\dot{y} - \dot{y}_d) + \lambda(y - y_d) \tag{11}$$

where

x, x_d, $\dot{x}$ = x position, desired x position, x velocity
y, y_d, $\dot{y}$ = y position, desired y position, y velocity
θ, θ_d, $\dot{\theta}$ = θ position, desired θ position, θ velocity

The control law for each degree of freedom is chosen so that the appropriate s^2 remains a Lyaponov function of the system subject to bounded disturbances and modelling errors. By using a time-varying boundary layer concept, the control laws avoid high frequency control actions that could excite unmodelled dynamics. The boundary layer concept is an interpolation of the control laws about the s=0 surface. The interpolation is made time-varying to achieve the optimum tradeoff between tracking error and parametric uncertainty along a desired trajectory. The basic philosophy behind sliding mode control is that when the system is outside an invariant region, the s=0 $\pm$ boundary layer surface,

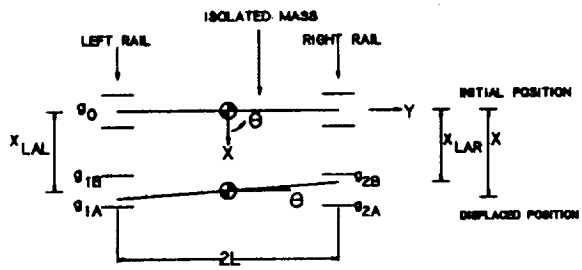

Figure 6. Testbed Kinematics

the control action is designed to be such that Eq. (12)

$$\frac{d}{dt} s^2 < 0 \tag{12}$$

or equivalently Eq. (13) ($\eta>0$)

$$\dot{s} < -\eta |s| \tag{13}$$

Fig. 7 shows that this control action will always move the system towards the boundary layer of the s=0 region. When s is positive, the time derivative of s is negative, when s is negative, the time derivative of s is positive. The system will reach the region within time constraints of the order of $1/\lambda$ where λ is the controller bandwidth. Once inside the boundary layer region, the tracking error in position and velocity remains bounded. The bounds on tracking error can be quantified in terms of modelling uncertainty, maximum disturbance bounds, desired trajectory parameters and system bandwidth. This relationship is called the "balance condition" and is discussed more in (5).

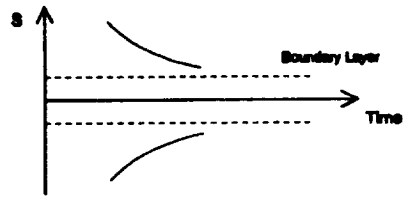

Figure 7. Sliding Mode Condition

The controller computes a set of two net control forces $F_{control\,x}$ and $F_{control\,y}$ and a net control torque $\tau_{control\,\theta}$. Then the currents are chosen to achieve this set of control actions. Notice that the choice of a set of 6 control currents to achieve three control actions is not unique. We chose the straightforward approach of using only one actuator of a given pair at a time. (For example if actuator 1A is on actuator 1B is off). This choice is acceptable

as long as the current controllers are designed to switch fast enough for the types of experimental tests to be run.

The net control force or torque for a particular degree of freedom has two components. One component is chosen as if the system were on the s=0 surface and the control action is to stay on the surface. This part of the control action is derived by making $\dot{s}$=0 and using the system model equations of motion. There is a feedfoward term and a term proportional to the velocity error. On the s=0, surface, this control action brings the tracking error to zero exponentially. The second component of control force or torque, the saturation function term, insures that ds^2/dt will remain decreasing outside the $s=0\pm\phi$ region in spite of disturbances and uncertainties.

$$F_{control\ y} = m_e\left(\ddot{y}_d + \lambda(\dot{y}_d - \dot{y}) + \overline{K_y}\ sat\left(\frac{s_y}{\phi_y}\right)\right)$$

$$F_{control\ x} = m_e\left(\ddot{x}_d + \lambda(\dot{x}_d - \dot{x}) + \overline{K_x}\ sat\left(\frac{s_x}{\phi_x}\right)\right) \qquad (14)$$

$$\tau_{control\ \theta} = I_e\left(\ddot{\theta}_d + \lambda(\dot{\theta}_d - \dot{\theta}) + \overline{K_\theta}\ sat\left(\frac{s_\theta}{\phi_\theta}\right)\right)$$

In Eq. (14), the K terms are dependent on the modelling uncertainty and the disturbance bounds. Also m_e and I_c are the assumed mass and moment of inertia respectively.

After the controller calculates the control forces and torque, it chooses a set of currents to achieve those forces Eq. (15-17).

$$F_{control\ x} - \frac{\tau_{control\ \theta}}{L_e} \geq 0:$$

$$I_{2A} = \sqrt{\frac{(g_{2A} + C_x)^2}{\alpha_{xe}}\left(F_{controlx} - \frac{\tau_{control\theta}}{L_e}\right)}$$

$$I_{2B} = 0$$

$$F_{control\ x} - \frac{\tau_{control\theta}}{L_e} < 0:$$

$$I_{2A} = 0$$

$$I_{2B} = \sqrt{\frac{-(g_{2B} + C_x)^2}{\alpha_{xe}}\left(F_{controlx} - \frac{\tau_{control\theta}}{L_e}\right)} \qquad (15)$$

$$F_{control\ x} + \frac{\tau_{control\theta}}{L_e} \geq 0:$$

$$I_{1A} = \sqrt{\frac{(g_{1A} + C_x)^2}{\alpha_{xe}}\left(F_{control\ x} + \frac{\tau_{control\ \theta}}{L_e}\right)}$$

$$I_{1B} = 0$$

$$F_{control\ x} + \frac{\tau_{control\ \theta}}{L_e} < 0:$$

$$I_{1A} = 0$$

$$I_{1B} = \sqrt{\frac{-(g_{1B} + C_x)^2}{\alpha_{xe}}\left(F_{controlx} + \frac{\tau_{control\ \theta}}{L_e}\right)}$$

(16)

$$F_{control\ y} \geq 0:$$

$$I_{3A} = \sqrt{\frac{2}{\alpha_{ye}}(g_{3A} + C_y)^2\ F_{control\ y}}$$

$$I_{3B} = 0$$

$$F_{control\ y} < 0:$$

$$I_{3A} = 0$$

$$I_{3B} = \sqrt{\frac{-2}{\alpha_{ye}}(g_{3B} + C_y)^2\ F_{control\ y}}$$

(17)

CONTROLLER ANALYSIS

Comparison of sliding mode and conventional controllers For comparison, a phase lead controller, typically used in magnetic suspension systems, was designed for the test-bed. Additionally, since the sliding mode controller has the advantage of having information about the desired trajectory which is used in a feedfoward path, a third controller was designed consisting of a linear phase lead controller and a nonlinear feedfoward term which utilized gap measurements and desired force. A block diagram of this controller is shown in Fig. 8.

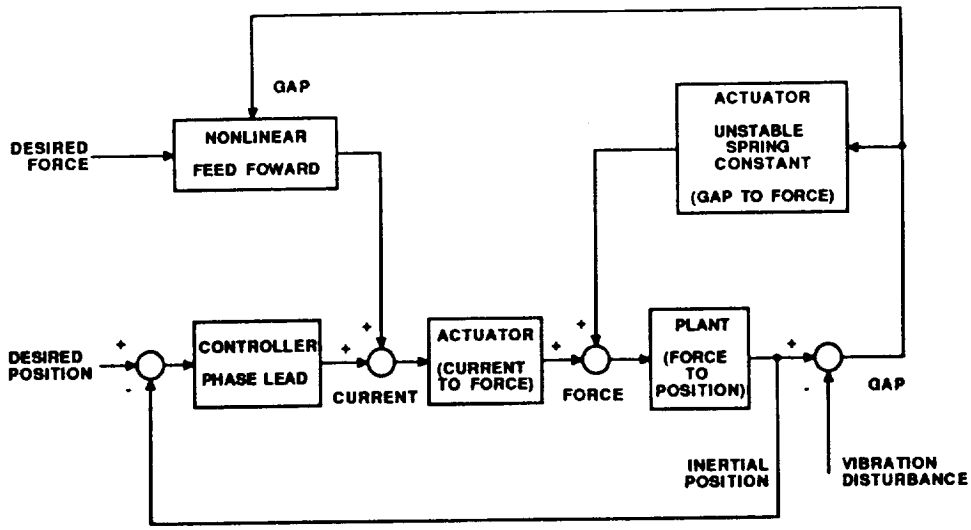

Figure 8. Block Diagram of Phase Lead with Feedforward Controller

The sliding mode bandwidth parameter (λ) and the closed loop bandwidth of the phase lead and phase lead with feedfoward were chosen to be 40 Hz. Simulations were run for the test scenarios which include a large amplitude, low frequency slewing maneuver and a small amplitude higher frequency angular disturbance. Performance measures of rms tracking error, stability margins and vibration disturbance attenuation were examined. Additionally, robustness of the three types of controllers to a particular type of modelling uncertainty was investigated.

Fig. 9 is a performance comparison plot of rms tracking error to a desired slew maneuver vs vibration disturbance amplitude. Both tracking error and vibration disturbance amplitude are normalized by the nominal gap. Perfect measurement and estimation systems are assumed. The slew maneuver is a 1 cm 5 Hz sinusoid and the vibration disturbance is an angular disturbance at 23 Hz. The magnitude of the angular vibration disturbance can be found using small angle approximations. This plot shows that the sliding mode controller has better tracking performance by two orders of magnitude than the phase lead controller. At very small disturbance amplitudes, the phase lead with feedfoward is comparable in tracking performance to the sliding mode controller, but this performance deteriorates significantly with larger disturbance amplitudes. Another interesting feature of this plot is that the sliding mode controller has higher stability margins than the other control approaches. The stability margin is reached when one or more of the magnetic gaps to go the zero. The plot shows that the phase lead and phase lead with feedfoward can handle disturbances up to about 20% and 30% of the nominal gap. This sliding mode controller can handle disturbances that are 90% of the nominal gap. Furthermore, this particular sliding mode controller was only designed to handle angular disturbances that were 50% of the nominal gap, the controller could easily be designed for higher disturbances in order to achieve even higher stability margins by trading off against tracking performance.

The ability of the sliding mode controller to operate near over the full range of it's magnetic gap is another advantage over linear controllers. Linear controllers, which are

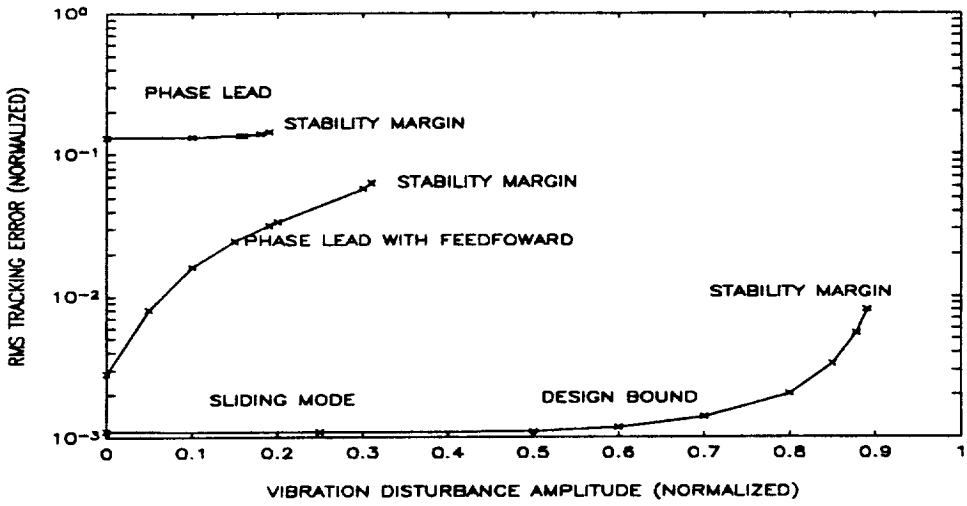

Figure 9. Controller Performance Comparison

biased about an operating current, can only operate in a reduced gap range to avoid attraction to one or the other biased actuator. The sliding mode controller has superior stability range and start-up capabilities.

Another performance measure to assess the potential of the sliding mode controller is vibration disturbance attenuation. This is a measure of how much disturbance energy is transmitted to the tracking body. Figure 10 shows vibration disturbance attenuation vs vibration disturbance frequency. The plot is again based on simulations a 1 cm 5 hz slew and a angular vibration disturbance. The magnitude of the angular disturbance is about .004 rad, which corresponds to approximately half the nominal gap when using small angle approximations. Vibration disturbance attenuation is defined to be the ratio in db of output angular disturbance energy to input angular disturbance energy. An alternative measure is disturbance attenuation at the disturbance frequency. This would be calculated by comparing the power spectral densities of the angular output response and the angular input disturbance. However, unlike linear systems, a nonlinear system can spread its response over the frequency domain. Due to this fact, the energy measure of vibration disturbance attenuation is preferred because it is a broadband measurement.

The sliding mode controller achieves better disturbance attenuation than the phase lead or the phase lead with feedfoward approaches. Performance at disturbance frequencies near the closed loop bandwidth is of particular interest because in this disturbance frequency range linear controllers have limited capability, as discussed earlier. For these simulations, analysis (Eq. 1) indicated the limiting value of isolation to be approximately -9 db for a phase lead controller. The plot shows that this limitation is accurate. The sliding mode controller, because of its different structure, is not limited to this performance value. It achieves about -40 db at disturbance frequencies near the closed loop bandwidth, a 30 db improvement over linear controllers. Using the balance condition, this isolation performance can be directly related to modelling accuracy, bandwidth and sampling time of the sliding mode controller.

Although this plot shows the sliding mode control has better performance than the

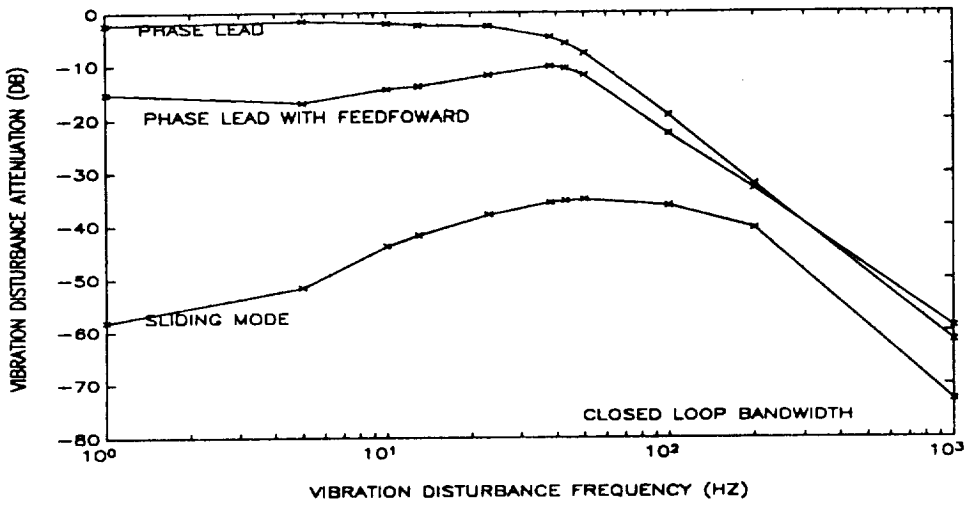

Figure 10. Controller Performance Comparison

other approaches at low disturbance frequencies, improved linearized control approaches can be designed by increasing the loop gain at low frequencies. This would result in a controller which had better disturbance attenuation at low frequencies than the phase lead and phase lead with feedfoward; however, it would still be limited at disturbance frequencies near the closed loop bandwidth.

Robustness to modelling uncertainty is an important capability for any control design. In the presence of parameter uncertainty, dynamic parameter variation, or model structure uncertainty, a robust controller maintains a specified level of performance and remains stable. For this type of actuator, the force proportionality to the current squared is a very good approximation; however, the force dependence on the gap is more uncertain. One reason for this modelling uncertainty is due to the curvature of the actuator target surfaces. Curvature is useful because it reduces cross-coupling between axes, however, it introduces a variation in gap. As discussed earlier, the force-gap-current models used in Eq. 4-6, are accurate to within 1% for gaps which ranged from plus or minus 50% of the nominal gap (7).

In order to investigate the effect of modelling uncertainty on controller performance and stability, we varied the force-gap-current proportionality term used in the controller models by plus or minus 10% of the value use in the plant simulation model. Fig. 11 is a plot of rms tracking error (normalized by the nominal gap value) as a function of modelling uncertainty in the force-gap-current proportionality term. The x axis is the ratio of the proportionality term used in the controller to the proportionality term used in the plant simulation model. A value of one indicates the controller is using a perfect model. These simulations were based on a 1 cm 5 hz sinusoidal slew in the presence of a 23 Hz .004 radian sinusoidal angular disturbance. The sliding mode controller has better tracking performance than the phase lead and the phase lead with feedfoward controllers when the uncertainty in the proportionality term ranges to plus or minus ten percent. However, these performance advantages are very sensitive to modelling uncertainty. Good modelling is essential for performance improvements to be realized.

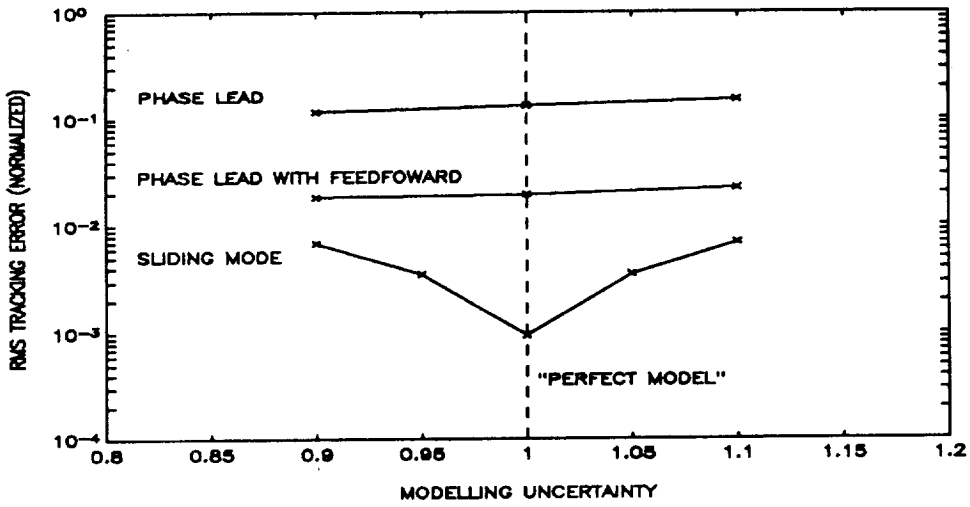

Figure 11. Controller Robustness Comparison

The Effects of Discrete Time, Estimation Errors, and Measurement Errors.

Realistic factors which will decrease the attainable performance of the system include effects due to the discrete time nature of the controller, finite word-length, measurement system imperfections, and estimation errors. The stability of the sliding mode controller with an estimation scheme has not been fully examined in the literature; however, simulations indicated that estimators can be designed for this system that do not seriously degrade performance or cause instability.

Controller currents are held constant over the sampling period. Additionally, due to control law computation time, there is a time delay between measurement of sensor data and control action. For this test-bed, the computation time is approximately 250 milliseconds. The sampling rate is 1000 Hz.

The measurement system errors include gap sensor nonlinearities and angular velocity sensor dynamics. The LVDT dynamics are high frequency effects and thus are neglected. The moving rails are under closed loop control and these effects are also negligible. The effects of sensor noise is not presented in this paper; they are expected to be negligible.

Fig. 12 shows a plot of the gap vs gap sensor voltage. The gap sensors were Mechanical Technology Incorporated ASP-50-ILA units with greater than 1 mm 1% linear range. The simulations used a third order fits to simulate the sensor. The estimation schemes considered also used third order fits to obtain gap from gap voltage.

Fig. 13 is the angular velocity sensor magnitude response vs frequency. The angular velocity sensor was an Applied Technology Associates magneto-hydrodynamic angular rate sensor (4). At low frequencies (less than .5 Hz), the angular velocity sensor magnitude response falls off. In this frequency range, any estimation scheme must utilize gap and LVDT rail measurements and the kinematic relations (Eq. 5-8).

The first estimation scheme presented here makes use of information from all of the sensors. At low frequencies, the inertial sensors do not provide good information, so

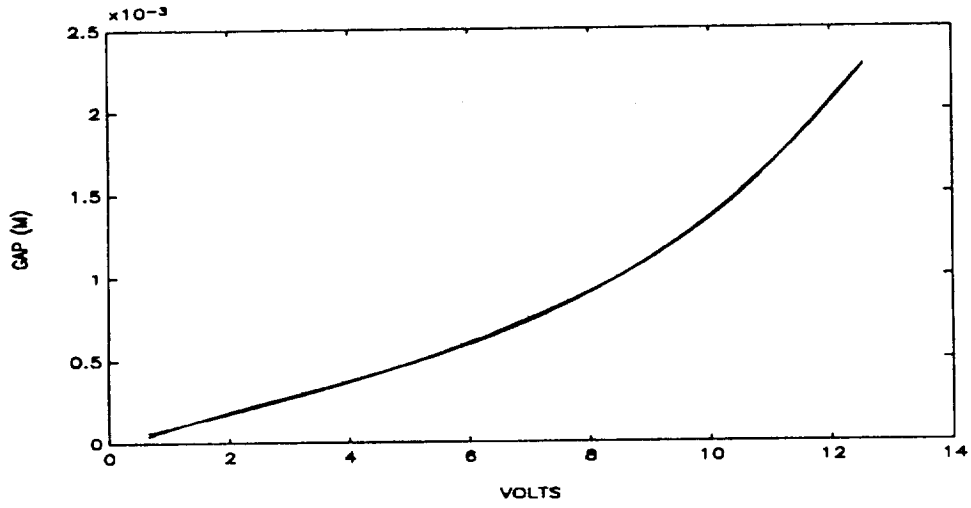

Figure 12. Gap Sensor Nonlinearity

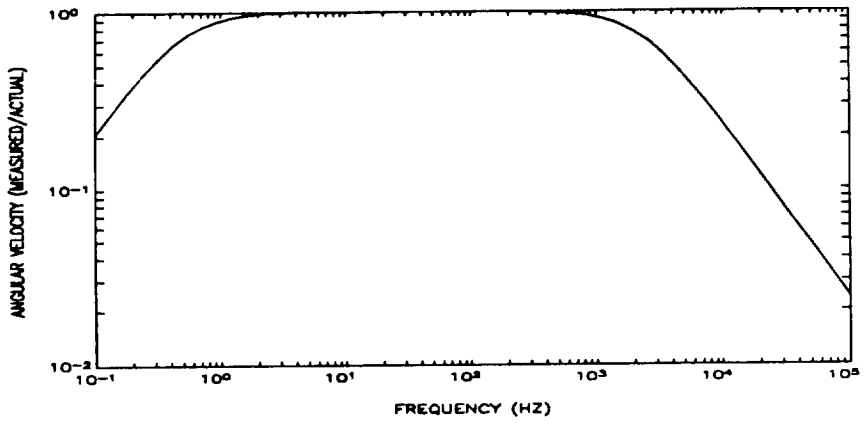

Figure 13. Angular Velocity Sensor Frequency Response

the gap sensors and LVDT measurements are used. The angular estimation filters have been designed to utilize angular velocity sensor information all the way down to its capacity at .5 Hz (Fig. 13). The angular position estimate uses mostly the low frequency estimate based on gaps and LVDT's for frequencies under 2 Hz. For simpler implementation, the x-axis filters in this particular estimator are using mostly low frequency information for x estimates. Future work should make better use of the accelerometer for inertial measurements; this requires low frequencies (compared to the sampling rate) in the estimation filter to remove the dc bias and was not considered in this phase of the work because of problems with implementation. Subsampling is one option to alleviate these numerical problems.

The first estimation scheme will not work in the testbed. The angular velocity sensor has too much broadband noise to get good angular position and velocity estimates. A second estimation scheme was designed which used only the gap and LVDT rail position measurements. The kinematic relationships are used (Eq. 5-8) to get estimates of angular and translational (x) position. The positions are then filtered to get velocity estimates.

Table 1 is based on a simulations of a 1 cm, 5 Hz slew with .0045 radian, 25 Hz angular vibration disturbance. The sliding mode controller bandwidth parameter is 40 Hz. The table shows three measures of performance: normalized rms tracking error, vibration disturbance attenuation at the vibration disturbance frequency, and broadband vibration disturbance attenuation. The performance measures are best with a perfect model, measurement system and estimation scheme. The rms tracking error is .16% of nominal gap and the vibration disturbance attenuation measures -35 and -33.8 db respectively. The effects due to modelling error are small. The effects of time delay between measurement and control action degrade tracking performance by an order of magnitude. Isolation performance is also reduced to about -30 db. The effect of estimation errors degrade tracking performance by an order of magnitude and do not significantly affect isolation performance. The second estimation scheme is tracking better than the first for this particular controller design. The effects of imperfect measurements, namely gap sensor nonlinearity and angular velocity sensor dynamics, also degrades tracking and does not significantly degrade isolation performance.

The effect of the estimator becomes more important with higher bandwidth controllers. For example, simulations of a 1 cm 5 Hz slew with a .0045 radian, 23 Hz angular disturbance with 160 Hz. bandwidth controller were performed. The perfect model, measurement and estimation case achieved -60 db of vibration isolation. The first estimation scheme, which utilized the inertial sensors measurements, had a performance reduction to -30 db of isolation when using perfect measurements. The second estimation scheme, which utilized only gap and rail measurements, was not adequate and the stability margin of the controller was reached.

HARDWARE RESULTS

To date, the testbed subcomponents have been tested and the testbed assembled and functionally tested. The sliding mode control algorithms have been implemented with a Texas Instruments TMS320-C25 digital signal processor coded directly in assembly language. Preliminary closed-loop tests were performed with a high bandwidth (160 Hz) controller in which the sliding mode control currents were reduced by a constant scaling factor. This factor was introduced because the current drives need to be modified to accept larger currents than originally specified.

Tests were performed in which the isolated mass was displaced by a full gap displacement and the desired position was the nominal centered position. Figure 14 shows the results of these experimental tests and two simulations. The modified simulation reflects the scaling of control currents and the gap sensor nonlinearity. The "perfect" simulation assumes perfect model, perfect measurement, perfect estimation and no current scaling factor. The rise time for the "perfect" simulation and for the experimental test are both about .075 seconds. The modified simulation takes about twice as long but reflects the oscillatory behavior about the final value. The modified simulation is very sensitive to scaling factor and the gap sensor nonlinearity fit.

TABLE 1.
The Effects of Discrete Time and Estimation Errors.

40 Hz Bandwidth Controller
1 cm 5 Hz slew
.0045 rad 25 Hz Disturbance

Effects	Comments	RMS Error / Nominal Gap	Vibration Disturbance Attenuation at Vibration Disturbance Frequency (db)	Vibration Disturbance Attenuation (db)
	Perfect Model Perfect Measurements Perfect Estimation No Time Delay	.0016	-35.0	-33.8
Modelling Error	1% Modelling Error Perfect Measurements Perfect Estimation No Time Delay	.002	-34.9	-33.7
Discrete Time	Perfect Model Perfect Measurements Perfect Estimation 1/4 sampling period delay (.0025 sec)	.05	-29.9	-28.6
Estimation Errors	Perfect Model Perfect Measurement No Time Delay			
	Estimator 1	.06	-34.9	-33.7
	Estimator 2	.03	-34.1	-32.9
Measure-ment and Estimation Errors	Perfect Model Imperfect Measurement No Time Delay			
	Estimator 1	.06	-33.5	-32.5
	Estimator 2	.03	-32.	-29.7

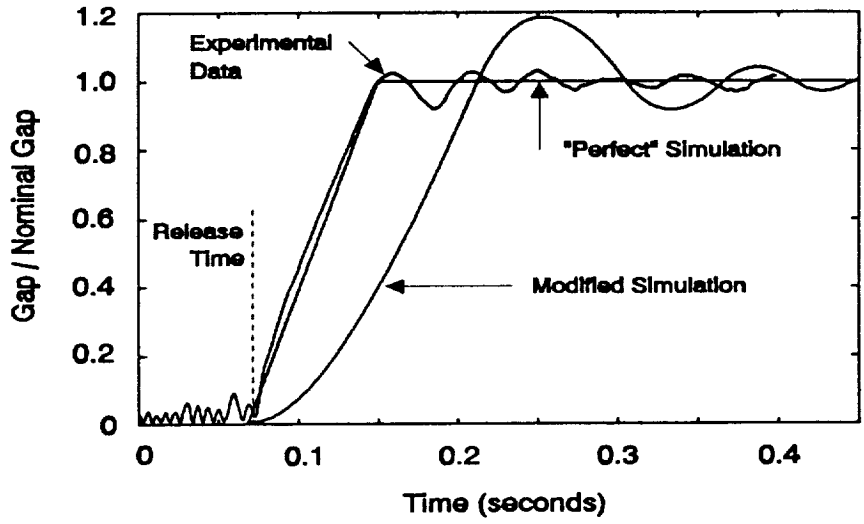

Figure 14. Initial Offset Test

Additionally, slew and angular vibration isolation tests with the hardware were performed for a 2.5 mm 1 Hz slew and single frequency angular disturbances ranging form .0009 to .003 radians up to 30 Hz. Vibration isolation measures of ranging from -23 to -36 db were observed for this range of disturbances. Simulation results were in the same range; however, they are very sensitive to the gap sensor nonlinearity which is not precisely known for the experimental tests that were run. After testbed modifications, we have since measured the gap sensor nonlinearity. Simulations presented earlier incorporate this nonlinearity. The next step in hardware verification is to increase the current drive capabilities. This will allow experimental comparisons to the simulations presented in this paper.

CONCLUSIONS AND RECOMMENDATIONS

Control algorithm development and system simulations have shown that sliding mode control is an attractive approach to providing precision tracking in the presence of disturbance vibrations. The sliding mode controller has a number of advantages over conventional designs. Most important is improved performance. For this testbed, the sliding mode controller can increase the vibration isolation while slewing by 30 db compared to a conventional control algorithm. Although controller performance improvements are very sensitive to actuator modelling accuracy, high levels of modelling accuracy can be achieved for aerospace applications by experimental testing.

Issues associated with the "real world" application of sliding mode control were investigated. Perhaps the most important was the incorporation of a state estimator with the sliding mode controller. System performance was depends on the quality of the measurements and the estimation scheme. A number of other estimator designs are now being investigated, including a linearized Kalman filter, extended (nonlinear) Kalman filter, and sliding mode observers (1,3,8). Estimation errors become more important as

the controller bandwidth is increased.

A laboratory testbed was designed and built and preliminary testing has been performed. Further testing is ongoing.

Recommendations for future research are to apply sliding mode control to an existing precision pointing and tracking application. This entails determining the modelling accuracy and computational requirements to meet the vibration isolation requirements of the particular application.

ACKNOWLEDGEMENTS

The research was conducted by SatCon Technology Corporation under Phase II Small Business Innovation Research (SBIR) Contract DASG60-88-C-0040 sponsored by the Strategic Defense Initiative Organization (SDIO) Innovative Science and Technology Office and managed by the U.S. Army Strategic Defense Command (ASDC) in Huntsville, AL. The authors would like to thank Dr. David Lukins and Dr. John Phillips of ASDC for their guidance.

REFERENCES

1 Misawa, E.A., Hedrick, J.K., "Nonlinear Observers-A State-of-the-Art Survey," ASME Journal of Dynamic Systems, Measurement and Control, III(3), Sept. 1989, pp. 344-352.

2 Slotine, J-J.E., "Sliding Controller Design for Non-Linear Systems," International Journal of Control, 40(2), 1984, pp. 421-434.

3 Yao, W.H. and Hedrick, J.K. "Nonlinear Adaptive Control of a Three Degree of Freedom Magnetic Suspension System,", Internal Report, Feb. 28, 1990, Department of Mechanical Engineering, Univ. of California, Berkeley, Calif.

4 "MHD Angular Motion Sensor Model IETL-001", Preliminary, Mar. 16, 1989, Applied Technology Associates, Inc., Albuquerque, NM.

5 Asada, H., Slotine, J.-J.E., "Trajectory Control," Robot Analysis and Control, 1st Ed., Wiley, New York, 1986, pp. 133-179.

6 AFAL/ARBH, Statement of Work, Space Active Vibration Isolation (SAVI), Kirtland AFB, NM, 1985.

7 Johnson,B.G., Misovec,K.M., Flynn,F., Anastas,G. Avakian,K.,Downer,J.,Gondahaleker,V.,Hockney, R., "Active Magnetic Vibration Isolation Using Sliding Mode Control", R06-90, Sept. 1990, SatCon Technology Corporation, Cambridge, MA.

8 Misovec, K.M. "A Comparison of Estimation Approaches for Use in a Sliding Mode Control Magnetic Vibration Isolation Testbed", to be published, Sept. 1990, SatCon Technology Corporation, Cambridge, MA.